C_{60}@Lysozyme: Direct Observation by Nuclear Magnetic Resonance of a 1:1 Fullerene Protein Adduct

Matteo Calvaresi,[†,*] Fabio Arnesano,[‡] Sara Bonacchi,[†] Andrea Bottoni,[†] Vincenza Calò,[‡] Stefano Conte,[†] Giuseppe Falini,[†,*] Simona Fermani,[†] Maurizio Losacco,[‡] Marco Montalti,[†] Giovanni Natile,[‡] Luca Prodi,[†] Francesca Sparla,[§] and Francesco Zerbetto[†,*]

[†]Dipartimento di Chimica "G. Ciamician", Alma Mater Studiorum Università di Bologna, via F. Selmi 2, 40126 Bologna, Italy, [‡]Dipartimento di Chimica, Università di Bari "A. Moro", via E. Orabona 4, 70125 Bari, Italy, and [§]Dipartimento di Farmacia e Biotecnologie, Alma Mater Studiorum Università di Bologna, via Irnerio 42, 40126 Bologna, Italy

ABSTRACT Integrating carbon nanoparticles (CNPs) with proteins to form hybrid functional assemblies is an innovative research area with great promise for medical, nanotechnology, and materials science. The comprehension of CNP–protein interactions requires the still-missing identification and characterization of the 'binding pocket' for the CNPs. Here, using Lysozyme and C_{60} as model systems and NMR chemical shift perturbation analysis, a protein–CNP binding pocket is identified unambiguously in solution and the effect of the binding, at the level of the single amino acid, is characterized by a variety of experimental and computational approaches. Lysozyme forms a stoichiometric 1:1 adduct with C_{60} that is dispersed monomolecularly in water. Lysozyme maintains its tridimensional structure upon interaction with C_{60} and only a few identified residues are perturbed. The C_{60} recognition is highly specific and localized in a well-defined pocket.

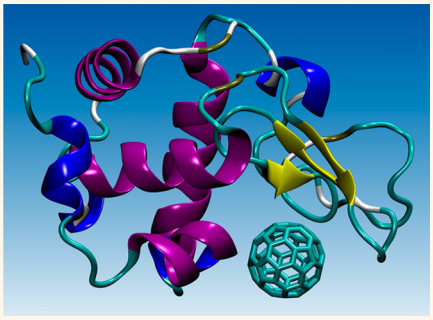

KEYWORDS: carbon nanoparticles · fullerene · lysozyme · nanobiotechnology · protein nanoparticle interaction · NMR spectroscopy

Access to adducts of carbon nanoparticles (CNPs) and proteins bears on a variety of areas that range from nanotechnology to nanomedicine to nanotoxicology.[1] From the point of view of nanotechnology, it is possible to use proteins to solvate[2] and even sort CNPs according to their morphology.[3] The combination of the peculiar properties of CNPs with those of proteins can also be used to create new functional materials exploitable to develop new biomedical and electronic devices, such as sensors.[4] In the context of nanomedicine, it may be possible to use fullerene as an innovative scaffold for drug design[5] or to use CNPs/protein hybrids to develop technologies for the simultaneous diagnosis, transport, and targeted delivery.[6] These nanoscale hybrids are able to assemble in an ordered and hierarchical manner[6] that can be used to develop new functional materials. In addition proteins can improve the dispersion of CNPs in nanocomposite, *e.g.*, for solar cells applications, preventing aggregation. The "dark side" of CNP–protein hybrids is the possibility that *in vivo* the CNPs presence alters the protein conformation and perturbs its functioning,[8] which may trigger unexpected biological reactions and/or lead to (nano-)toxicity.[9]

The full comprehension of CNP–protein interactions requires the still-missing identification and characterization of the 'binding pocket' for the CNPs. Once known, it could offer the possibility of guiding the design of new hybrid materials where the interaction is enhanced or diminished.

To simplify the problem, we focus on C_{60} interaction with proteins.[10] This fullerene can be considered a representative model system for CNPs, in general, but at the same time it offers the opportunity to work with a well-characterized system.

The ability of C_{60} to interact with proteins was demonstrated for the first time by pioneering work that reported its inhibiting activity on HIV-proteases.[11] Protein interaction of fullerene-based compounds was later identified in other proteins as proteases,[12] anti-Buckminsterfullerene antibody

* Address correspondence to matteo.calvaresi3@unibo.it, giuseppe.falini@unibo.it, francesco.zerbetto@unibo.it.

Received for review December 10, 2013 and accepted January 22, 2014.

Published online January 22, 2014
10.1021/nn4063374

Fab fragment,[13] acetylcolinesterase,[14] human and bovine serum albumin,[15,16] lysozyme,[17] *etc.*[18−32]

To date, the identification of the fullerene binding site in these proteins, and the subsequent protein structural and functional modifications, has relied only on indirect techniques.[8−32] As a rule, tryptophan quenching and computational studies are put to hard work when trying to identify unambiguously a binding site. Infrared spectroscopy, circular dichroism and other spectroscopic techniques can monitor changes in the secondary structure of proteins, but give only limited information at the level of individual amino acids. Activity assays are *per se* also partly informative if the binding site of the CNP is unknown, since direct inhibition, allosteric effects or perturbation of the enzyme structure can all be responsible for changes in the enzyme activity. To complicate matters, it is not clear if the measured effects rely on (i) the formation of a 1:1 adduct, (ii) binding of the protein with fullerene aggregates, or (iii) average effects deriving by the binding of fullerene/fullerenes to multiple protein binding sites.

Here, for the first time, using NMR chemical shift perturbation analysis, a protein−CNP binding pocket is identified unambiguously in solution and the effect of the binding, at the level of the single amino acid, is characterized by a variety of experimental and computational approaches. As a model protein we choose lysozyme (LSZ). It is one of the less expensive, more deeply understood, and most used proteins in research (it is very resistant and stable, easy to modify genetically to create mutants, very simple to crystallize and perfectly known from the biological point of view). Lysozyme is the ideal workhorse to unravel the underlying principles of protein structure, function, dynamics, and folding.

NMR can provide high-resolution information on protein structure and changes occurring in protein−CNP complexes formed in aqueous environment. Chemical shift perturbation (CSP) is a well-established technique used to monitor protein−ligand,[33] protein−protein,[34] and protein−nanoparticle[35] interactions. Two-dimensional $^{1}H-^{15}N$ NMR experiments are used to detect, at the atomic level, the interaction between LSZ and C_{60}. The NMR investigation is complemented with spectroscopic studies and activity assays that for the first time can be interpreted on the basis of the knowledge of the C_{60}@LSZ interaction site.

RESULTS AND DISCUSSION

C_{60}@Lysozyme. Proteins and LSZ, in particular, are able to disperse pristine single-wall nanotubes in water with the aid of ultrasonication.[2,3] A similar approach is used to create a hybrid C_{60}@LSZ complex (see Methods section). The UV−visible spectrum of C_{60}@LSZ (Figure 1) revealed features that belong to both components of the adduct, showing the distinctive absorption of

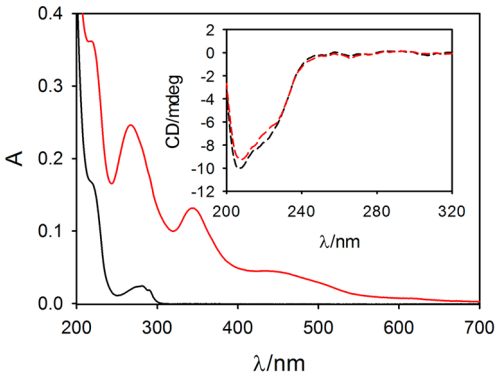

Figure 1. Spectroscopic characterization of C_{60}@LSZ hybrid. UV−visible spectra of monomeric LSZ protein (black line) and purified C_{60}@LSZ hybrid (red line). The inset shows the circular dichroism spectra of monomeric LSZ (black line) and C_{60}@LSZ hybrid (red line).

fullerene (341 nm) and protein (281 nm). On the basis of the photophysical data reported for fullerene,[36] the absorbance is compatible with a concentration of solubilized C_{60} quite similar to that of lysozyme as expected in the case of the formation of a stable 1:1 complex between the two species. To explore whether the interaction of LSZ with C_{60} causes a conformational change in the protein, we performed circular dichroism measurements (inset Figure 1). The global structure of the protein is only slightly perturbed upon binding. SDS-PAGE (Figure S1) and size exclusion chromatography (Figure S2) revealed that LSZ is in a monomeric form, thus excluding, respectively, covalent and noncovalent aggregation phenomena that could occur in the ultrasonication process.

NMR Chemical Shift Perturbation Analysis. Two-dimensional $^{1}H-^{15}N$ NMR experiments were used to detect changes in the chemical environment of all coupled H and N atoms of the protein upon formation of protein complexes (chemical shift perturbation analysis, CSP). Figure 2 shows the superposition of 2D $^{1}H,^{15}N$ HSQC spectra of free LSZ and C_{60}@LSZ hybrid. Each cross-peak represents a NH group of the protein backbone (one per amino acid residue, excluding Pro residues) and of a Trp indole ring. Cross-peaks, corresponding to NH_2 groups of Asn and Gln side chains, are also present. Even after complex formation the spectral resolution remains very high, indicating that the protein retains its folding.

Only a few NH backbone groups undergo significant change in chemical shift upon binding to C_{60}, with the majority of them remaining unaffected. This finding indicates that the interaction of C_{60} with LSZ is very specific and affects only a few amino acids.

The chemical shift perturbation for each amide NH group of the protein backbone is shown in Figure 3a. The residues that undergo the largest changes, not contiguous in the sequence, cluster in a specific region of the three-dimensional structure of the protein (Figure 3b). These residues (4, 19, 43−46, 50−54,

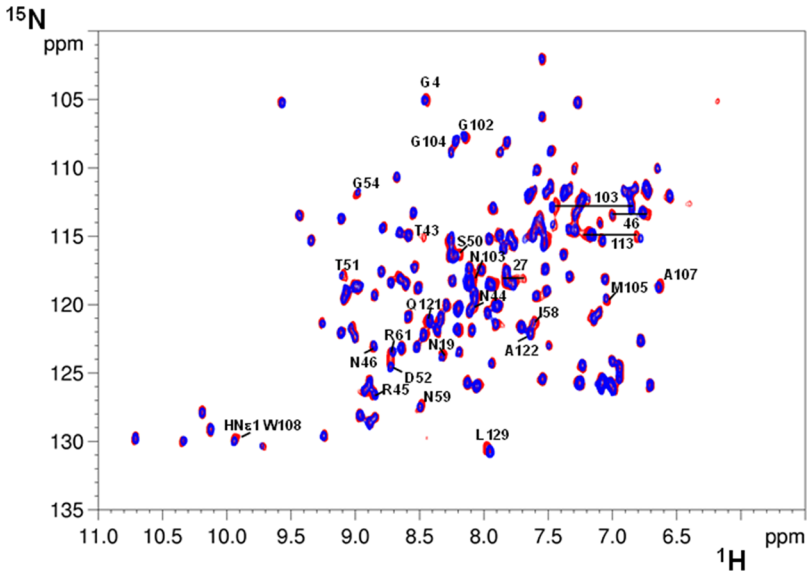

Figure 2. Superposition of 2D $^{1}H,^{15}N$ HSQC spectra of samples of free LSZ (blue) and C_{60}@LSZ hybrid (red). Black labels indicate cross-peak assignment of residues undergoing chemical shift perturbation upon interaction with C_{60}.

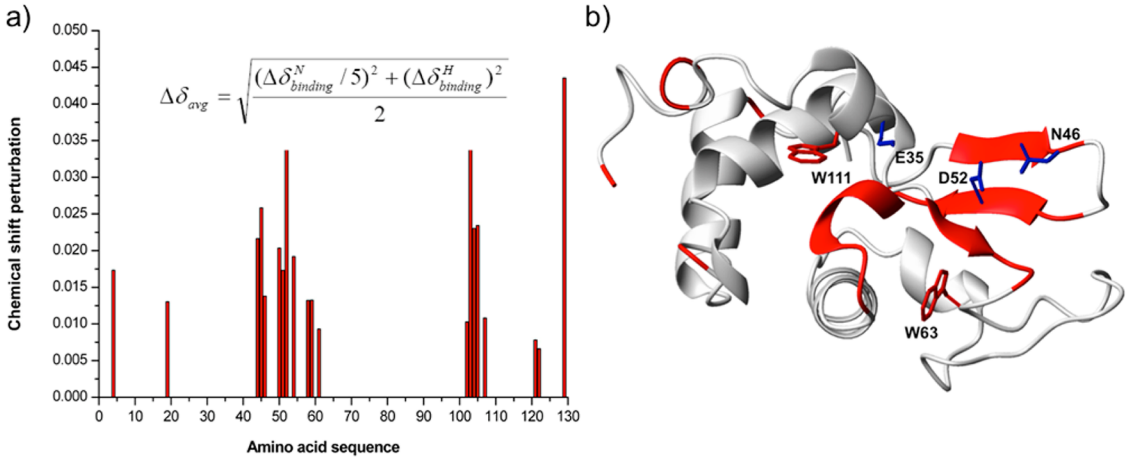

Figure 3. NMR chemical shift perturbation analysis of LSZ upon interaction with C_{60}. (a) CSP is given by the weighted average chemical shift differences $\Delta\delta_{avg}$(HN) of cross-peaks in the $^{1}H,^{15}N$ HSQC spectra of free and bound LSZ (see equation embedded in the figure). (b) 3D representation of the residues undergoing chemical shift changes (red region) upon C_{60} binding.

58−61, 102−107, 121−122, 129) are most likely involved in the interaction with C_{60}. The chemical shift of the NH group of Trp 108 indole ring (HNε1) is also sensitive to complex formation (Figure 3a).

A docking protocol[10,25] recently validated to detect fullerene protein binding pockets identifies the same region of the NMR as the most likely binding site. In Figure 4a the C_{60} localization resulting from the docking calculations and the residues undergoing the largest chemical shift changes identified by NMR are mapped on the 3D structure of LSZ (red area).

LSZ structure consists of two domains (α and β). The α domain contains residues 1−35 and 85−129 (four α helices and a short 3_{10} helix), while the β domain contains residues 36−84 (a triple-stranded antiparallel β sheet, a long loop, and a 3_{10} helix). C_{60} is wedged in the cleft between the α and β domains (Figure 4b), in proximity of the catalytic site.

Fluorescence Spectroscopy. The fluorescence spectrum of LSZ upon excitation at 280 nm shows an emission band with a maximum at 334 nm and a fluorescence quantum yield Φ = 0.28. The emission is due to the presence of six tryptophan residues. The fluorescence of LSZ overlaps with the electronic transition of C_{60} at 341 nm.[36] The corresponding excited state of C_{60} is expected to quench the emission of the protein *via* fluorescence resonant energy transfer (FRET). As a consequence, the complexation of C_{60} may be confirmed by the quenching of the Trp fluorescence (Figure 5a).

Steady-state and time-resolved fluorescence spectra were analyzed taking into account the position of

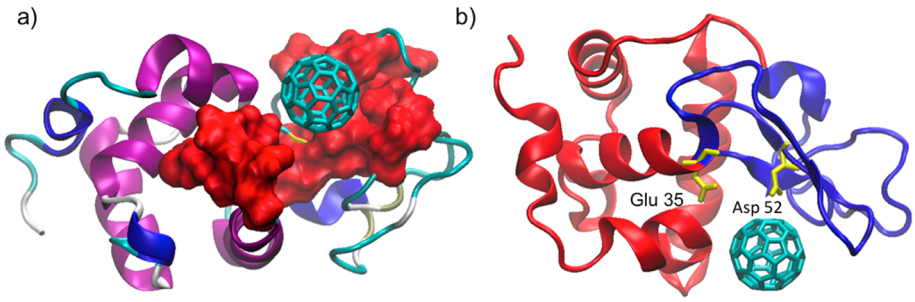

Figure 4. Identification of the C_{60} binding pocket. (a) Docking of C_{60} in the LSZ structure; the red area corresponds to the residues undergoing the largest chemical shift changes in the NMR measurements; (b) LSZ α (red) and β domains (blue). The active site residues (Glu35 and Asp 52), critical for the catalytic activity of the enzyme, are shown in yellow.

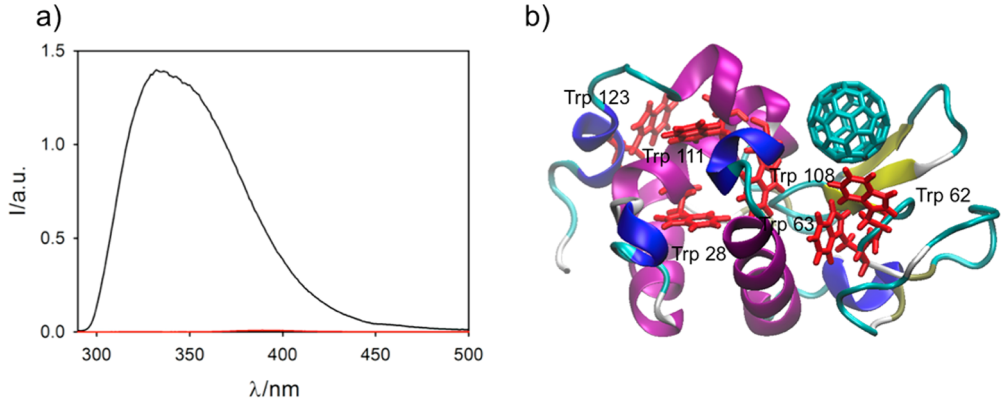

Figure 5. Quenching of the LSZ fluorescence by C_{60}. (a) Steady-state fluorescence ($\lambda_{excitation}$ = 280 nm) of solutions of monomeric LSZ (black line) andC_{60}@LSZ hybrid (red line); (b) TRP locations in the LSZ structure.

C_{60} binding site. The main emitters, responsible for more than 80% of LSZ fluorescence, are Trp62 and Trp108.[37,38] C_{60} binds in their proximity. In comparison to free LSZ, Figure 5a shows that, in the spectrum of C_{60}@LSZ, Trp fluorescence is almost completely quenched. Time correlated single photon counting (TCSPC) experiments allowed to investigate the quenching process in more detail.

The excited state decay of pristine LSZ was fitted by a triexponential model ($\chi^2 = 1.025$).[37,38] The associated lifetimes were $\tau_1 = 2.73$ ns ($f_1 = 0.20$), $\tau_2 = 1.37$ ns ($f_2 = 0.42$) and $\tau_3 = 0.46$ ns ($f_3 = 0.38$),[37,38] where $f_i = B_i/(B_1 + B_2 + B_3)$ is the population of the emitter, and B_i is the pre-exponential term relative to the lifetimes τ_i; τ_1 and τ_2 were attributed to Trp62 and Trp108, respectively, while τ_3 was attributed to the convolution of the other four tryptophans present in LSZ.[37,38] Upon inclusion of C_{60}, the excited state decay is dominated by a very fast component $\tau_1' \sim 0.1$ ns ($f_1 = 0.99$). Two residual components $\tau_2' = 2.92$ ns ($f_2 = 0.003$) and $\tau_3' = 1.17$ ns ($f_3 = 0.007$) due to a small fraction (~1%) of uncomplexed LSZ can be still detected. These results demonstrate that about 99% of LSZ in solution hosts a C_{60} in a 1:1 adduct.

To investigate the origin of the residual emission, we first calculated the distance between donors (the tryptophan residues) and acceptor (C_{60}) at which the efficiency, η_{RET}, of energy transfer is 0.5. This distance is conventionally called Föster radius, r_0, and depends on the spectral properties of donor and acceptor. The value we found is $r_0 = 30.2$ Å. As shown in the Methods section, it can be used to calculate the actual distance between the donor and the acceptor once η_{RET} is known. According to the Föster model, the shortest and predominant component of the excited state lifetime, $\tau_1' \sim 0.1$ ns, is relative to the tryptophan residues closest to C_{60}. Assuming that these residues are Trp62 and Trp108, we determined $\eta_{RET} \sim 0.97$ and $\eta_{RET} \sim 0.91$, which imply a distance from C_{60} of $r = 16.9$ and 20.5 Å (see Methods). Notice that η_{RET} depends on the excited state lifetime of the nonquenched residues.

The calculated distances are not consistent with those (considerably smaller) resulting from the NMR analysis and the docking calculations, which are 8.8 and 9.3 Å. We deduce that the excited tryptophan molecules that decay with $\tau_1' \sim 0.1$ ns are not Trp62 and Trp108 but the other TRP residues further away from C_{60} (see Figure 5b). Similar considerations apply to the other two components of the decay $\tau_2'$and τ_3' that are due to the poorly quenched Trp units more distant from C_{60}. On the basis of these observations, we conclude that the fluorescence of Trp62 and Trp108 is quenched to such an extent to become undetectable by the time-resolved measurements of our experimental conditions.

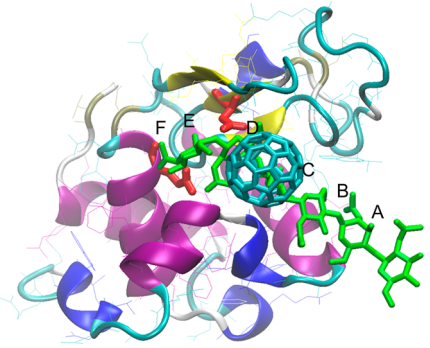

Figure 6. Binding of C_{60} in the LSZ substrate binding pocket. Superposition of C_{60} with a NAG_6 lysozyme substrate analogue, PDB file 1SFG,[40] where the NAG_6 molecule is bound to sites ABCDE, leaving the F site empty with the remaining saccharide ring located in a solvent region adjacent to the A site. In red, catalytic residues Glu35 and Asp 52. LSZ cleaves the glycosidic bond connecting ring "D" to ring "E".

Determination of Enzyme Activity. Since C_{60} binds in proximity of the catalytic site, the activity of free LSZ and C_{60}@LSZ was determined fluorimetrically by following the glycolysis of 4-methylumbelliferyl β-D-*N*,*N*′,*N*″-triacetylchitotrioside (a fluorogenic substrate that has been used for the detection of lysozyme, peptidoglycan, muramidase, and endochitinase activity, see Figure S3).[39] The activity is quantified by monitoring the release of 4-methylumbelliferone after 30 min of incubation. The C_{60}@LSZ retains 53% of activity of the free enzyme. This finding can be explained by considering that in its activity LSZ hydrolyzes a number of structurally similar substrates, such as alternating polysaccharide copolymers of *N*-acetyl glucosamine (NAG) and *N*-acetyl muramic acid (NAM) (Figure S3). LSZ cleaves the $\beta(1-4)$ glycosidic linkage, connecting the C1 carbon of NAM to the C4 carbon of NAG. The active site of LSZ consists of six subsites, designated as "**A**" to "**F**", that can accommodate six sugar moieties (Figure 6). LSZ preferentially cleaves the glycosidic bond connecting ring "**D**" to ring "**E**". C_{60} binds to the saccharide binding sites "**C**", which clogs the binding site of the substrate, making difficult its binding, without completely inhibiting its activity (Figure 6). Functionalization of the fullerene cage, to make it more hydrophilic and/or charged, offers the possibility to modulate its inhibitory activity, as observed in similar systems.[14,32]

CONCLUSION

NMR and spectroscopic data show, unequivocally and for the first time, that it is possible for LSZ to form a stoichiometric 1:1 adduct with C_{60}. Circular dichroism indicates that LSZ maintains its tridimensional structure upon interaction with C_{60}. Chemical shift perturbation (CSP) analysis confirms that the 3D structure remains largely unaffected by the C_{60} binding, and only a few well-identified residues are perturbed. The C_{60} recognition is highly specific and localized by NMR in a well-defined pocket. Enzyme activity assays show that C_{60}@LSZ retains 53% of activity of the free enzyme.

Several consequences of these findings can be envisaged. LSZ provides a simple way to disperse pristine C_{60} in water in monomolecular form in alternative to well-known macrocyclic receptors.[41] Knowledge of the specific recognition pocket of LSZ for C_{60} may also allow the design of new functionalization patterns of the cage able to modulate the interactions of CNPs with LSZ. Notice that LSZ recognition pocket of fullerene is different from LSZ recognition pocket of carbon nanotubes.[42,43] Therefore, in principle, LSZ, and possibly other proteins, could be used to sort different CNPs or to assemble them in a controlled way.

Establishment of a simple procedure to prepare and characterize protein−CNP hybrids can be used in the future to (i) improve the coupling between the two types of moieties for sensor or for targeting application,[44] or (ii) to use fullerene and fullerene derivative as innovative scaffolds for inhibiting compounds.[5] It can also be envisaged that the procedure can be used to develop functionalized CNPs with smaller interactions and reduce the toxicological risk connected to the exposition to CNPs.[45]

METHODS

C_{60}@Lysozyme Preparation. C_{60}@LSZ hybrid was prepared by addition of C_{60} powder (Sigma-Aldrich, code 572500, used as commercially available, without any additional purification), in 2:1 excess with respect to the stoichiometric relationship, to 3 mL of a 10^{-3} M solution of LSZ (Sigma-Aldrich, code L6876) in Milli-Q water.

After sonication for 60 min using a probe tip sonicator (Misonix XL2020; 500 W, 40% power) in an ice bath, C_{60} was dispersed in the LSZ solution forming a dark brown mixture. A dark-brown solution was obtained after centrifugation at 5000*g* for 10 min and collection of the supernatant. These conditions were optimized to maximize the concentration of C_{60}@Lysozyme in water, at the same time avoiding aggregation, therefore, affording homogeneous and stable solutions.

Gel Electrophoresis. The aggregation state of LSZ upon interaction with C_{60} was monitored by SDS-PAGE. Briefly, samples of LSZ (500 μM), prepared either in the absence or in the presence of C_{60}, were mixed with an equal volume of Laemmli buffer. Each sample was boiled for 5 min. Samples were loaded on 15% polyacrylamide gels and run in TGS 1× buffer at 100 V. After running the gel was silver stained.

Size Exclusion Chromatography. Samples of LSZ (500 μM), prepared either in the absence or in the presence of C_{60}, were analyzed by SEC using an AKTA Purifier UPC900 FPLC instrument (GE Healthcare) equipped with a Superdex 75 10/300GL column (GE Healthcare). An elution buffer of 50 mM sodium phosphate, pH 7.0, containing 150 mM NaCl was used. The flow rate was 0.5 mL/min. The UV detector was set at 280 nm. With the use of SEC calibration standards (Sigma-Aldrich), the peak eluting at 15 mL was consistent with the molecular weight of LSZ (14.4 kDa).

Nuclear Magnetic Resonance Spectroscopy. NMR experiments were performed at 25 °C on 3.0 mM samples of unlabeled LSZ

in 10% D_2O, in the presence or absence of C_{60}. The C_{60}@LSZ complex was prepared as described above. Natural abundance 2D ^1H,^{15}N-edited HSQC spectra were collected on a Bruker Avance 600 spectrometer using a triple-resonance probe equipped with pulsed field gradients along the *z*-axis. HSQC spectra were acquired using a gradient-enhanced sequence in which coherence selection and water suppression are achieved *via* gradient pulses. A total of 512 transients were acquired over an F2 (^1H) spectral width of 14 ppm into 2048 complex data points for each of 256 t_1 increments in TPPI mode with an F1 (^{15}N) spectral width of 40 ppm centered at 118 ppm. The sequence was optimized with an INEPT delay 1/(4JNH) of 2.78 ms. A recycle delay of 1.0 s was used. Decoupling during the acquisition time was achieved using a GARP scheme. Data zero-filled in F1 were subjected to apodization using a squared cosine bell function in both dimensions prior to Fourier transformation and phase correction. Data were processed using the Bruker software TOPSPIN and analyzed with the program CARA (The Computer Aided Resonance Assignment Tutorial, R. Keller, 2004, CANTINA Verlag). Resonance assignment of LSZ was performed using available chemical shifts data (BMRB Entry 4831) with the aid of 2D TOCSY and NOESY, and 3D ^{15}N-edited NOESY spectra. Chemical shift changes upon complex formation with C_{60} were reported as weighted average chemical shift differences $\Delta\delta_{avg}$(HN) to account for differences in spectral widths between ^1H and ^{15}N resonances. $\Delta\delta_{avg}$(HN) were calculated as described elsewhere[46] (*i.e.*, $\Delta\delta_{avg}(HN) = [(\Delta\delta H^2 + (\Delta\delta N/5)^2)/2]^{1/2}$, where $\Delta\delta H$ and $\Delta\delta N$ are chemical shift differences for ^1H and ^{15}N, respectively) and plotted as a function of the protein sequence.

Photophysical Measurements. Photophysical studies were carried out in ultrapure water solutions (Milli-Q system by Millipore was used for water purification). The LSZ and C60@LSZ solutions were kept refrigerated at 4 °C. To perform photophysical measurements, the solutions were diluted to 2:300 with pure water. UV−vis absorption spectra were recorded at 25 °C by means of Perkin-Elmer Lambda 45 spectrophotometer. The fluorescence spectra were recorded with an Edinburgh FLS920 fluorimeter equipped with a photomultiplier Hamamatsu R928P. The same instrument connected to a PCS900 PC card was used for the Time Correlated Single Photon Counting (TCSPC) experiments.

Circular dichroism spectra were obtained with a Jasco J-810 spectropolarimeter.

The Föster distance r_0, at which the efficiency of energy transfer is $\eta_{RET} = 0.5$, is calculated from the spectral data according to eq 1.

$$r_0 = 9.78 \times 10^3[\kappa^2 n^{-4} \Phi_D J(\lambda)]^{1/6} \text{ (Å)} \quad (1)$$

where $\kappa^2 = 2/3$ is an orientation factor, n is the refractive index, Φ_D is the fluorescence quantum yield of the donor and $J(\lambda)$ is the spectral overlap according to eq 2.

$$J(\lambda) = \int f_D(\lambda)\epsilon_A(\lambda)\lambda^4 \, d\lambda \quad (2)$$

where $\epsilon_A(\lambda)$ is the molar absorption coefficient of the acceptor and f_D is the normalized fluorescence spectrum of the donor obtained from the experimental one $F_D(\lambda)$ according to eq 3.

$$f_D(\lambda) = \frac{F_D(\lambda)}{\int F_D(\lambda)\, d\lambda} \quad (3)$$

Equation 4 was used to calculate the average tryptophan−C_{60} distance r in case that τ_1' was related either to the decay of Trp62 ($\eta_{RET} \sim 0.97$) or of Trp108 ($\eta_{RET} \sim 0.91$)

$$\eta_{RET} = \frac{r_0^6}{r^6 + r_0^6} \quad (4)$$

Activity Assay. The activities of LSZ and of C_{60}@LSZ were measured following the release of 4-methylumbelliferone from the substrate 4-methylumbelliferyl β-D-*N*,*N*′,*N*″-triacetylchitotrioside hydrate (Sigma-ALdrich, code M5639). A stock solution of 87 μM 4-methylumbelliferyl β-D-*N*,*N*′,*N*″-triacetylchitotrioside hydrate was prepared following the manufacturer's instruction. The substrate concentration was calculated from the absorbance at 316 nm (molar extinction coefficient of 12.3 mM^{-1}). Two-milliliters sample solutions were prepared mixing either 27.4 μL of 1 mM LSZ or 27.4 μL of 1 mM C_{60}@LSZ with 1.7 μL of 87 μM substrate in 25 mM ammonium acetate buffer, pH 4.6, and the solutions were incubated for 30 min at 42 °C. The reactions were stopped by adding 240 μL of NaOH 1 N. The release of free 4-methylumbelliferone was recorded by emission fluorescence spectra (Spectrofluorimeter Jasco FP-770), using an exciting wavelength of 360 nm and measuring the emission at 455 nm.

Conflict of Interest: The authors declare no competing financial interest.

Acknowledgment. This work was supported by the Italian "Ministero dell'Università e della Ricerca" (FIRB 2011 – Rete Integrata per la Nano Medicina, RBAP114AMK, RINAME Project). We also thank the Universities of Bari and Bologna, and the Consorzio Interuniversitario di Ricerca in Chimica dei Metalli nei Sistemi Biologici (CIRCMSB).

Supporting Information Available: SDS-PAGE, size exclusion chromatography and LSZ substrates (natural and the one used in the activity assay) representation. This material is available free of charge *via* the Internet at http://pubs.acs.org.

REFERENCES AND NOTES

1. Calvaresi, M.; Zerbetto, F. The Devil and Holy Water: Proteins and Carbon Nanotubes Hybrids. *Acc. Chem. Res.* **2013**, *46*, 2454–2463.
2. Nepal, D.; Geckeler, K. E. pH-Sensitive Dispersion and Debundling of Single-Walled Carbon Nanotubes: Lysozyme as a Tool. *Small* **2006**, *2*, 406–412.
3. Nie, H.; Wang, H.; Cao, A.; Shi, Z.; Yang, S.-T.; Yuan, Y.; Liu, Y. Diameter-Selective Dispersion of Double-Walled Carbon Nanotubes by Lysozyme. *Nanoscale* **2011**, *3*, 970–973.
4. Choi, Y.; Moody, I. S.; Sims, P. C.; Hunt, S. R.; Corso, B. L.; Perez, I.; Weiss, G. A.; Collins, P. G. Single-Molecule Lysozyme Dynamics Monitored by an Electronic Circuit. *Science* **2012**, *335*, 319–324.
5. Da Ros, T.; Prato, M. Medicinal Chemistry with Fullerenes and Fullerene Derivatives. *Chem. Commun.* **1999**, *8*, 663–669.
6. Kostarelos, K.; Bianco, A.; Prato, M. Promises, Facts and Challenges for Carbon Nanotubes in Imaging and Therapeutics. *Nat. Nanotechnol.* **2009**, *4*, 627–633.
7. Grigoryan, G.; Kim, Y. H.; Acharya, R.; Axelrod, K.; Jain, R. M.; Willis, L.; Drndic, M.; Kikkawa, J. M.; DeGrado, W. F. Computational Design of Virus-like Protein Assemblies on Carbon Nanotube Surfaces. *Science* **2011**, *332*, 1071–1076.
8. Park, K. H.; Chhowalla, M.; Iqbal, Z.; Sesti, F. Single-Walled Carbon Nanotubes are a New Class of Ion Channel Blockers. *J. Biol. Chem.* **2003**, *278*, 50212–50216.
9. Zuo, G.; Kang, S.-G.; Xiu, P.; Zhao, Y.; Zhou, R. Interactions Between Proteins and Carbon-Based Nanoparticles: Exploring the Origin of Nanotoxicity at the Molecular Level. *Small* **2013**, *9*, 1546–1556.
10. Calvaresi, M.; Zerbetto, F. Baiting Proteins with C_{60}. *ACS Nano* **2010**, *4*, 2283–2299.
11. Friedman, S. H.; DeCamp, D. L.; Sijbesma, R.; Srdanov, G.; Wudl, F.; Kenyon, G. L. Inhibition of the HIV-1 Protease by Fullerene Derivatives: Model Building Studies and Experimental Verification. *J. Am. Chem. Soc.* **1993**, *115*, 6506–6509.
12. Tokuyama, H.; Yamago, S.; Nakamura, E.; Shiraki, T.; Sugiura, Y. Photoinduced Biochemical Activity of Fullerene Carboxylic Acid. *J. Am. Chem. Soc.* **1993**, *115*, 7918–7919.
13. Braden, B. C.; Goldbaum, F. A.; Chen, B. X.; Kirschner, A. N.; Wilson, S. R.; Erlanger, B. F. X-ray Crystal Structure of an Anti-Buckminsterfullerene Antibody Fab Fragment: Biomolecular Recognition of C_{60}. *Proc. Natl. Acad. Sci. U.S.A.* **2000**, *97*, 12193–12197.
14. Pastorin, G.; Marchesan, S.; Hoebeke, J.; Da Ros, T.; Ehret-Sabatier, L.; Briand, J.-P.; Prato, M.; Bianco, A. Design

and Activity of Cationic Fullerene Derivatives as Inhibitors of Acetylcholinesterase. *Org. Biomol. Chem.* **2006**, *4*, 2556–2562.
15. Belgorodsky, B.; Fadeev, L.; Ittah, V.; Benyamini, H.; Zelner, S.; Huppert, D.; Kotlyar, A. B.; Gozin, M. Formation and Characterization of Stable Human Serum Albumin-tris-Malonic Acid [C_{60}] Fullerene Complex. *Bioconjugate Chem.* **2005**, *16*, 1058–1062.
16. Belgorodsky, B.; Fadeev, L.; Kolsenik, J.; Gozin, M. Formation of a Soluble Stable Complex between Pristine C_{60}-Fullerene and a Native Blood Protein. *ChemBioChem* **2006**, *7*, 1783–1789.
17. Yang, S.-T.; Wang, H.; Guo, L.; Gao, Y.; Liu, Y.; Cao, A. Interaction of Fullerenol with Lysozyme Investigated by Experimental and Computational Approaches. *Nanotechnology* **2008**, *19*, 395101.
18. Kim, J. E.; Lee, M. Fullerene Inhibits β-Amyloid Peptide Aggregation. *Biochem. Biophys. Res. Commun.* **2003**, *303*, 576–579.
19. Wolff, D. J.; Barbieri, C. M.; Richardson, C. F.; Schuster, D. I.; Wilson, S. R. Trisamine C_{60}-Fullerene Adducts Inhibit Neuronal Nitric Oxide Synthase by Acting as Highly Potent Calmodulin Antagonists. *Arch. Biochem. Biophys.* **2002**, *399*, 130–141.
20. Mashino, T.; Shimotohno, K.; Ikegami, N.; Nishikawa, D.; Okuda, K.; Takahashi, K.; Nakamura, S.; Mochizuki, M. Human Immunodeficiency Virus-Reverse Transcriptase Inhibition and Hepatitis C Virus RNA-Dependent RNA Polymerase Inhibition Activities of Fullerene Derivatives. *Bioorg. Med. Chem. Lett.* **2005**, *15*, 1107–1109.
21. Innocenti, A.; Durdagi, S.; Doostdar, N.; Strom, T. A.; Barron, A. R.; Supuran, C. T. Nanoscale Enzyme Inhibitors: Fullerenes Inhibit Carbonic Anhydrase by Occluding the Active Site Entrance. *Biorg. Med. Chem.* **2010**, *18*, 2822–2828.
22. Kraszewski, S.; Tarek, M.; Treptow, W.; Ramseyer, C. Affinity of C_{60} Neat Fullerenes with Membrane Proteins: A Computational Study on Potassium Channels. *ACS Nano* **2010**, *4*, 4158–4164.
23. Ratnikova, T. A.; Govindan, P. N.; Salonen, E.; Ke, P. C. *In Vitro* Polymerization of Microtubules with a Fullerene Derivative. *ACS Nano* **2011**, *5*, 6306–6314.
24. Wu, H.; Lin, L. N.; Wang, P.; Jiang, S. S.; Dai, Z.; Zou, X. Y. Solubilization of Pristine Fullerene by the Unfolding Mechanism of Bovine Serum Albumin for Cytotoxic Application. *Chem. Commun.* **2011**, *47*, 10659–10661.
25. Calvaresi, M.; Zerbetto, F. Fullerene Sorting Proteins. *Nanoscale* **2011**, *3*, 2873–2881.
26. Liu, S. F.; Sui, Y.; Guo, K.; Yin, Z. J.; Gao, X. B. Spectroscopic Study on the Interaction of Pristine C_{60} and Serum Albumins in Solution. *Nano. Res. Lett.* **2012**, *7*, 433.
27. Govindan, P. N.; Monticelli, L.; Salonen, E. Mechanism of Taq DNA Polymerase Inhibition by Fullerene Derivatives: Insight from Computer Simulations. *J. Phys. Chem. B* **2012**, *116*, 10676–10683.
28. Monticelli, L.; Barnoud, J.; Orlowskid, A.; Vattulainen, I. Interaction of C_{70} Fullerene with the Kv1.2 Potassium Channel. *Phys. Chem. Chem. Phys.* **2012**, *14*, 12526–12533.
29. Kang, S. G.; Huynh, T.; Zhou, R. H. Non-Destructive Inhibition of Metallofullerenol Gd@C_{82}(OH)$_{22}$ on WW Domain: Implication on Signal Transduction Pathway. *Sci. Rep.* **2012**, *2*, 957.
30. Mentovich, E.; Belgorodsky, B.; Gozin, M.; Richter, S.; Cohen, H. Doped Biomolecules in Miniaturized Electric Junctions. *J. Am. Chem. Soc.* **2012**, *134*, 8468–8473.
31. Kang, S. G.; Zhou, G.; Yang, P.; Liu, Y.; Sun, B.; Huynh, T.; Meng, H.; Zhao, L.; Xing, G.; Chen, C.; *et al.* Molecular Mechanism of Pancreatic Tumor Metastasis Inhibition by Gd@C_{82}(OH)$_{22}$ and its implication for *de Novo* Design of Nanomedicine. *Proc. Natl. Acad. Sci. U.S.A.* **2012**, *109*, 15431–15436.
32. Durdagi, S.; Supuran, C. T.; Strom, T. A.; Doostdar, N.; Kumar, M. K.; Barron, A. R.; Mavromoustakos, T.; Papadopoulos, M. G. *In Silico* Drug Screening Approach for the Design of Magic Bullets: A Successful Example with Anti-HIV Fullerene Derivatized Amino Acids. *J. Chem. Inf. Model.* **2009**, *49*, 1139–1143.
33. Pellecchia, M.; Sem, D. S.; Wuthrich, K. NMR in Drug Discovery. *Nat. Rev. Drug Discovery* **2002**, *1*, 211–219.
34. Zuiderweg, E. R. P. Mapping Protein−Protein Interactions in Solution by NMR Spectroscopy. *Biochemistry* **2002**, *41*, 1–7.
35. Calzolai, L.; Franchini, F.; Gilliland, D.; Rossi, F. Protein-Nanoparticle Interaction: Identification of the Ubiquitin−Gold Nanoparticle Interaction Site. *Nano Lett.* **2010**, *10*, 3101–3103.
36. Guldi, D. M.; Prato, M. Excited-State Properties of C_{60} Fullerene Derivatives. *Acc. Chem. Res.* **2000**, *33*, 695–703.
37. Imoto, T.; Forster, L. S.; Rupley, J. A.; Tanaka, F. Fluorescence of Lysozyme: Emissions from Tryptophan Residues 62 and 108 and Energy Migration. *Proc. Natl. Acad. Sci. U.S.A.* **1971**, *69*, 1151–1155.
38. Formoso, C.; Forster, L. S. Tryptophan Fluorescence Lifetimes in Lysozyme. *J. Biol. Chem.* **1975**, *250*, 3738–3745.
39. Yang, Y.; Hamaguchi, K. Hydrolysis of 4-Methylumbelliferyl N-Acetyl-Chitotrioside Catalyzed by Hen and Turkey Lysozymes. pH Dependence of the Kinetics Constants. *J. Biochem.* **1980**, *87*, 1003–1014.
40. Von Dreele, R. B. Binding of N-Acetylglucosamine Oligosaccharides to Hen Egg-White Lysozyme: A Powder Diffraction Study. *Acta Crystallogr.* **2005**, *D61*, 22–32.
41. Canevet, D.; Pérez, E. M.; Martín, N. Wraparound Hosts for Fullerenes: Tailored Macrocycles and Cages. *Angew. Chem., Int. Ed.* **2011**, *50*, 9248–9259.
42. Asuri, P.; Bale, S. S.; Pangule, R. C.; Shah, D. A.; Kane, R. S.; Dordick, J. S. Structure, Function, and Stability of Enzymes Covalently Attached to Single-Walled Carbon Nanotubes. *Langmuir* **2007**, *23*, 12318–12321.
43. Calvaresi, M.; Hoefinger, S.; Zerbetto, F. Probing the Structure of Lysozyme-Carbon-Nanotube Hybrids with Molecular Dynamics. *Chem.—Eur. J.* **2012**, *18*, 4308–4313.
44. Goldsmith, B. R.; Mitala, J. J., Jr.; Josue, J.; Castro, A.; Lerner, M. B.; Bayburt, T. H.; Khamis, S. M.; Jones, R. A.; Brand, J. G.; Sligar, S. G.; *et al.* Biomimetic Chemical Sensors Using Nanoelectronic Readout of Olfactory Receptor Proteins. *ACS Nano* **2011**, *5*, 5408–5416.
45. Ali-Boucetta, H.; Nunes, A.; Sainz, R.; Herrero, M. A.; Tian, B.; Prato, M.; Bianco, A.; Kostarelos, K. Asbestos-Like Pathogenicity of Long Carbon Nanotubes Alleviated by Chemical Functionalization. *Angew. Chem., Int. Ed.* **2013**, *52*, 2274–2278.
46. Garrett, D. S.; Seok, Y. J.; Peterkofsky, A.; Clore, G. M.; Gronenborn, A. M. Identification by NMR of the Binding Surface for the Histidine-Containing Phosphocarrier Protein HPr on the N-Terminal Domain of Enzyme I of the Escherichia Coli Phosphotransferase System. *Biochemistry* **1997**, *36*, 4393–4398.